Korean J. Chem. Eng., 33(4), 1489-1499 (2016)
DOI: 10.1007/s11814-015-0245-1

pISSN: 0256-1115
eISSN: 1975-7220

Pt and Pt-Sn nanoparticles decorated conductive polymer-biowaste ash composite for direct methanol fuel cell

Dakshinamoorthy Prasanna and Vaithilingam Selvaraj†

Nanotech Research Lab, Department of Chemistry, University College of Engineering Villupuram,
(A Constituent College of Anna University, Chennai), Kakuppam, Villupuram, 605 103, Tamilnadu, India
(*Received 25 June 2015 • accepted 17 November 2015*)

Abstract−The present work is focused on the synthesis of platinum (Pt)and platinum-tin (Pt-Sn) nanoparticles decorated poly(aniline)-rice husk ash (PANI-RHA) composite by the chemical reduction of their respective metal salts. The obtained Pt/PANI-RHA and Pt-Sn/PANI-RHA composites were characterized by FT-IR, XRD, SEM, EDAX and HR-TEM analysis. Platinum nanoparticles were also decorated on RHA and PANI for comparative studies. The synthesized electrocatalysts have been subjected to electrooxidation of methanol by cyclic voltammetry. It has been concluded that the Pt nanoparticles decorated PANI-RHA composite exhibits a remarkable enhancement for the electrochemical oxidation of methanol when compared with Pt/PANI and Pt/RHA composites. So, PANI-RHA composite has proven to be a good supporting material for alcohol fuel cell applications. Further, Pt-Sn bimetallic nanoparticles decorated PANI-RHA composite exhibit a remarkable enhancement for the electrochemical oxidation of methanol compared to that of Pt/PANI-RHA catalyst. Hence, the above results suggest that Pt-Sn/PANI-RHA composite is a potent and low cost electrocatalyst for fuel cell industries.

Keywords: Platinum, Platinum-tin, Poly(aniline)-Rice Husk Ash, Electrooxidation, Methanol

INTRODUCTION

Electrooxidation of methanol at low temperature could enhance the commercialization of direct methanol fuel cell (DMFC) compared to that of other fuel cells. The methanol has characteristic advantages over other fuels in that they have higher theoretical mass energy density, zero or low pollutant emission, simple design, convenient for fuel transportation, storage and supply [1-3]. The complete electrooxidation of methanol involves six electrons. But, for small scale applications, like powering electronic devices and electric vehicles, direct alcohol fuel cells (DAFCs) have required durability and reliability. Platinum is a popular electrocatalyst for alcohol fuel cells because of its tremendous catalytic activity. However, methanol oxidation on a Pt electrode in acid medium can occur with the adsorption of CO species as poisonous intermediate, which can reduce the catalytic activity of the catalyst [4-7]. Furthermore, the high price of platinum still remains the major difficulty in the commercialization of DAFCs. So, platinum was combined with other low cost metals that have been widely investigated as electrocatalyst to decrease the Pt content [8-15], which can reduce the fabrication cost of fuel cells.

The electro-catalytic activity of supported catalysts is greater than that of unsupported catalysts [16]. So, the selection of a suitable supporting material is a key factor that may affect the performance of supported electrocatalysts owing to their interaction between metal particles and supporting materials. The active surface area of the supported electrocatalyst [17,18] has been enhanced due to the synergic effect obtained through the interaction between metal nanoparticles and supporting materials. Rice husk ash (RHA) is a renewable biomass, which is also chemically stable and resistant to thermal decomposition. Rice husk ash (RHA) plays an important role as supporting material for industrial applications such as oxidation of cyclohexane, cyclohexene and cyclohexanol [19,20]. In addition, the iron-incorporated rice husk ash is used as a catalyst for benzylation of toluene and xylene [21,22]. Due to these unique characteristics, RHA material has been proposed as a novel electrocatalyst support for fuel cell applications.

Conductive polymers were used as good supporting materials for fuel cell and solar cell applications. Among other conducting polymers, poly(aniline) (PANI) is known for its excellent properties such as high conductivity, stable chemical performance, small pore size, large surface area etc. Hence, the potential applications of the conducting polymers are making researchers focus on broad areas such as organic light-emitting diodes [23,24], transistors [25,26], solar cells [27,28], pH-sensors [29], biosensors [30], rechargeable batteries, membranes [31], electro-chromic displays [32], corrosion protecting coating [33] and fuel cells [34-38].

The present work has been proposed to prepare composite containing poly(aniline) (PANI) and rice husk ash (RHA) through the chemical oxidation method. RHA and PANI-RHA materials were characterized by Fourier transform infrared spectroscopy (FT-IR). The present work is focused on the development of mono (Pt) and bimetallic (Pt-Sn) nanoparticles deposited rice husk ash-poly(aniline)(PANI-RHA) composite. Pt nanoparticles deposited on naturally obtain rice husk ash and poly(aniline) have been pre-

†To whom correspondence should be addressed.
E-mail: vaithilingamselvaraj@gmail.com, vselva@aucev.edu.in, rajselva_77@yahoo.co.in

pared to prove that PANI-RHA is a good supporting material compared to that of PANI and RHA materials. The metal nanoparticles deposited on PANI-RHA composite have been characterized by various analytical methods such as X-ray diffraction (XRD), energy dispersive X-ray analysis (EDX), elemental mapping and transmission emission spectroscopy (TEM). The obtained Pt deposited RHA, PANI and PANI-RHA nanocomposites have been utilized for electrooxidation of methanol in acidic medium for comparative studies. Pt-Sn deposited PANI-RHA composite has been prepared to improve the catalytic activity as well as to reduce the total cost of the fuel cell constructions. The cyclic voltammetry results indicate that the Pt deposited PANI-RHA composite shows enhanced catalytic activity when compared with Pt/RHA and Pt/PANI composites, suggesting that the PANI-RHA is a good supporting material for methanol electrooxidation. It has also been noticed that the Pt-Sn system exhibits enhanced catalytic activity when compared to that of Pt deposited PANI-RHA nanocomposite. Hence, the above results suggest that the platinum-tin/PANI-RHA composite is a potent and low cost electrocatalyst for alcohol fuel cell applications.

EXPERIMENTAL METHODS

1. Chemicals and Materials

$H_2PtCl_6 \cdot 6H_2O$ (99%), $SnCl_2 \cdot 2H_2O$ (99%), sodium borohydride ($NaBH_4$), ammonium persulfate ($(NH4)_2S_2O_8$), sulfuric acid (H_2SO_4) and aniline (C_6H_7N) were purchased from SRL, India. Distilled water was used throughout the experiments and all experiments were carried out at 25 °C.

2. Preparation of Rice Husk Ash (RHA) and Poly(aniline)-Rice Husk Ash (PANI-RHA) Composite

The metal nanoparticle decorated poly(aniline)-rice husk ash was prepared according to Scheme 1. Rice husk was collected from a local rice mill, Pathirakottai, Tamilnadu, India and washed several times with de-ionized (DI) water and then dried in the sun for seven days. The dried rice husk was air burned and the resultant residue was crushed into fine powder (RHA). 40 grams of RHA powder was immersed in 1,000 mL of HCl (1M) solution for 4-6 h [39]. The acid treated RHA was washed several times with DI water and then dried in an oven at 110 °C for two days. The dried RHA was calcined in a muffle furnace at 350 °C for 6 h. Finally, the calcined rice husk ash was crushed into fine powder and stored in a desiccator. Before using RHA, it should be dried at 110 °C for 24 h.

Rice husk ash was functionalized using aniline monomer and ammonium persulfate as oxidant at 0-5 °C in an acidic medium (0.1 M HCl). In detail, 1 g of RHA was dispersed in 150 mL of 0.1 M HCl solution and 1 mL of aniline monomer in 100 mL of HCl solution was added to the above reaction mixture. To this reaction mixture, 0.82 g of $(NH_4)_2S_2O_8$ in 50 mL of HCl solution was added slowly with constant stirring over a temperature range of 0-5 °C. Then the reaction was continued for further 4 h at 25 °C. Finally, the PANI-RHA composite was filtered and its impurities were removed by washing several times with distilled water and dried at 60 °C in an oven for 24 h.

3. Synthesis of Mono and Bimetallic Nanoparticles Decorated PANI-RHA Nanocomposite

Pt-Sn/PANI-RHA catalyst was synthesized by the chemical reduction method using sodium borohydride as reducing agent. In this approach, 100 mg of PANI-RHA is dispersed in 50 mL of $NaBH_4$ solution (200 mg). To this, 52 mg (1 m·mol) of hexachloroplatinic acid and 22 mg (1 m·mol) of tin chloride dissolved in 50 ml of distilled water were added slowly in drop-wise under constantly stirring conditions. The stirring was continued for another 4 h to complete the reduction of metal ions. Finally, the solid was centrifuged, washed with distilled water and dried at 60 °C. By following similar procedure Pt/RHA, Pt/PANI and Pt/PANI-RHA electrocatalysts were synthesized for comparative studies.

4. Fabrication of Metal Nanoparticles Decorated PANI-RHA Electrodes

Graphite electrodes were used as the substrates for the synthesized metal/PANI-RHA catalysts. For the fabrication of Pt-Sn/PANI-RHA electrode, 5 mg of catalysts are dispersed in 100 μL of 0.05% Nafion solution and isopropanol (1 : 1) solution. A measured volume (25 μL) of this mixture was dropped on the top surface of the graphite electrode by using micropipette. The modified

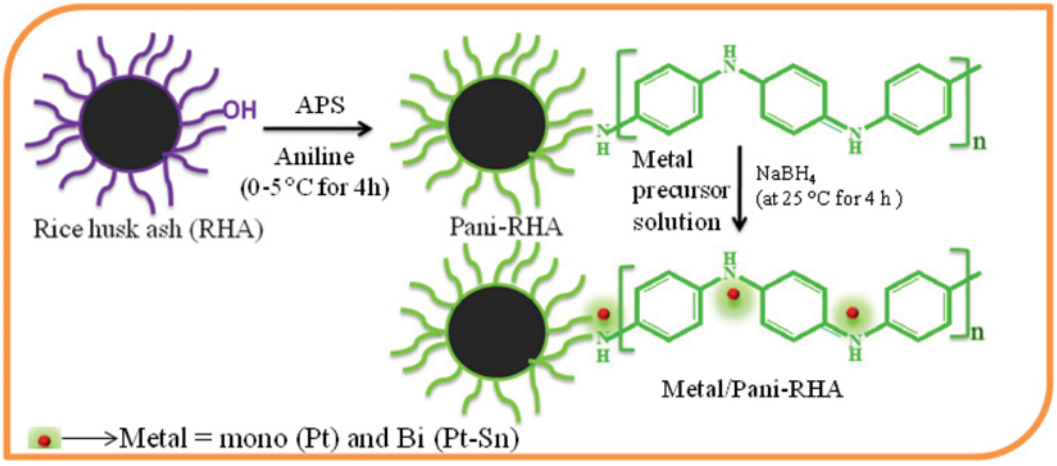

Scheme 1. The schematic representation of metal decoration on poly(aniline)-rice husk ash composite.

electrode was employed as the working electrode for the electrooxidation of methanol. Pt/RHA, Pt/PANI and Pt/PANI-RHA electrodes were also fabricated by following the above procedure.

5. Characterization

The IR spectra of RHA and PANI-RHA materials were recorded on an FT-IR spectrometer with Thermo Nicolet Model: 6700. While X-ray powder diffraction (XRD) was carried out on a Purkinjie diffractometer. The particle size and morphology of electrocatalysts were analyzed by high resolution transmission electron microscopy (HRTEM, JEOL 2010F). The elemental composition of metal nanoparticles present in the catalyst materials was performed using an energy dispersive X-ray analysis (EDX: Peltier cooled X-ray head from Thermo). The electrical conductivity was measured on compressed pellets using a resistance meter (Advantest) by four-probe method.

6. Electrochemical Measurements

Electrocatalytic activity and stability of all the catalysts were characterized by using cyclic voltammetry (CV) and chronoamperometry (CA) techniques for electrooxidation of methanol in acidic medium. The electrochemical measurements were conducted by using a multichannel electrochemical workstation with inbuilt FRA system (Biologic SAS, Model VSP2) in a conventional three-electrode test cell at 25 °C. Mono and bimetallic nanoparticles decorated PANI-RHA composites were used as the working electrode. The platinum and saturated calomel electrode (SCE) were used as counter and reference electrodes, respectively. Electrochemical impedance spectroscopy (EIS) was measured in 0.5 M H_2SO_4.

RESULTS AND DISCUSSION

1. FT-IR Analysis

Surface examination of RHA and PANI-RHA materials involved the Fourier transform infrared (FT-IR) spectrophotometer to confirm the formation of functional groups on RHA material. From the FT-IR spectrum (Fig. 1) of PANI-RHA, the characteristic functional groups such as -N-H and C-N appeared at 3,225 cm^{-1} and 1,305 cm^{-1}, respectively. The aromatic C=C stretching vibrations were visualized at 1,570 and 1,489 cm^{-1} [40-43], which confirmed the presence of poly(aniline) on the surface of RHA material. This implies that the rice husk ash has been successfully functionalized with aniline and the above peaks were absent in the case of rice husk ash material (Fig. 1). The presence of -NH groups on the surface of the rice husk ash is an advantage for uniform dispersion of metal particles on the surface of the poly(aniline)-rice husk ash composite.

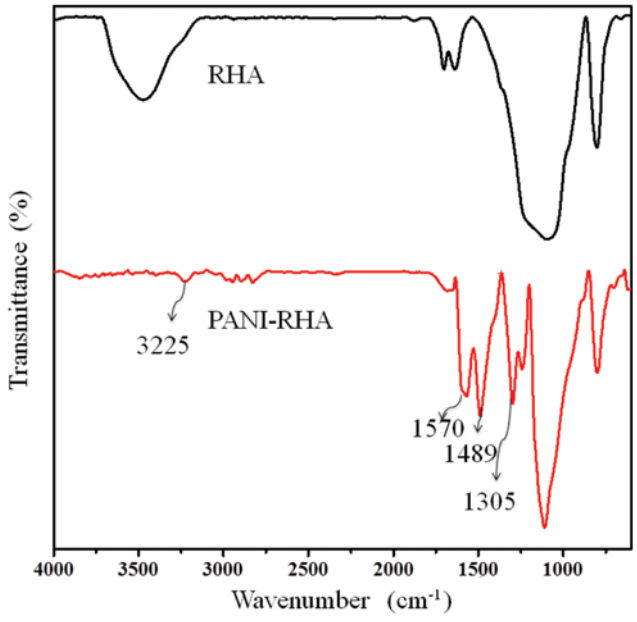

Fig. 1. FT-IR spectra of RHA and PANI-RHA materials.

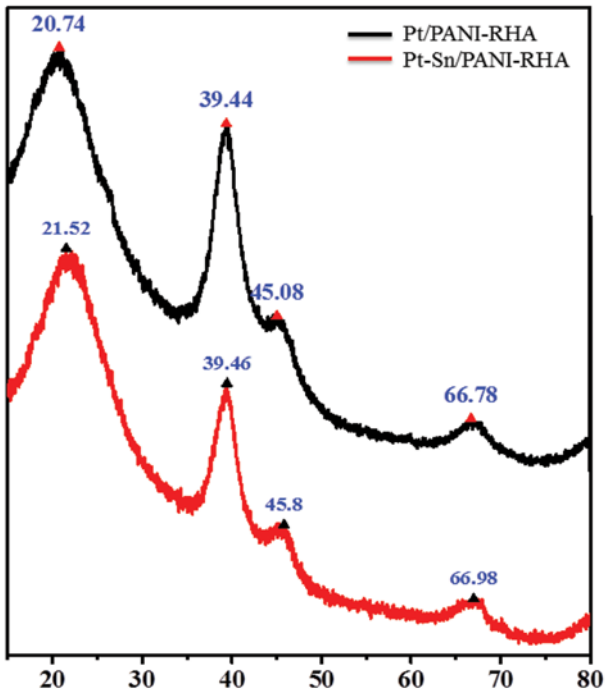

Fig. 2. XRD patterns of Pt/PANI-RHA and Pt-Sn/PANI-RHA electrocatalysts.

2. XRD Analysis

Fig. 2 shows the XRD patterns of the poly(aniline)-rice husk ash supported Pt and Pt-Sn electrocatalysts. A broad peak was visualized between 15 and 25° for both the electrocatalyst, which can confirm the amorphous nature of PANI-RHA composite. The face-centered-cubic (fcc) crystallographic structure of Pt (PCPDF file No. 87-0646) and its corresponding reflection planes (1 1 1), (2 0 0) and (2 2 0) were observed at 39.3°, 45.5° and 67.4°, respectively (Fig. 2) [44,45]. For Pt-Sn/PANI-RHA electrocatalyst, the reflection planes match very well with PCPDF file No. 07-0371 data of Pt-Sn, which are in good agreement with the previous literature report [46,47]. From Fig. 2, the Pt-Sn/PANI-RHA electrocatalyst has smaller positive peak shift when compared to that of Pt/PANI-RHA electrocatalyst. This is because platinum ions in the lattice structure were replaced by tin ions since there was not much difference in the ionic radius of Pt^{+2} (0.625 Å) and Sn^{+2} (0.69 Å).

3. Transmission Electron Microscopy (TEM)

Figs. 3 and 4 show the HRTEM images of synthesized Pt/PANI-RHA and Pt-Sn/PANI-RHA nanocomposites. The size dis-

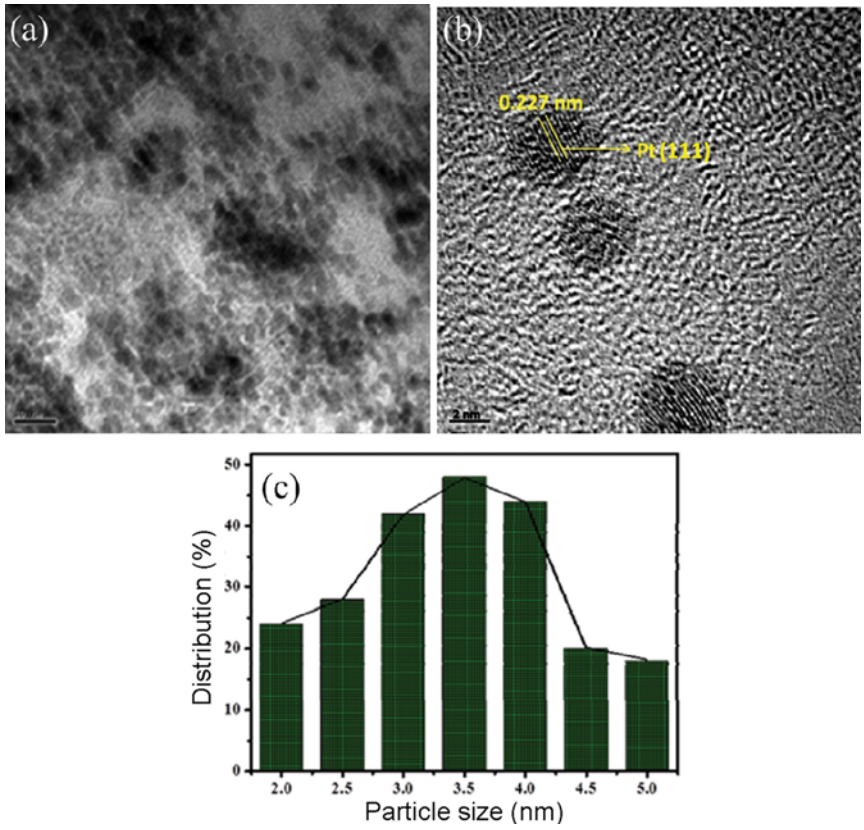

Fig. 3. HRTEM images and size distribution histogram of Pt/PANI-RHA nanocatalyst.

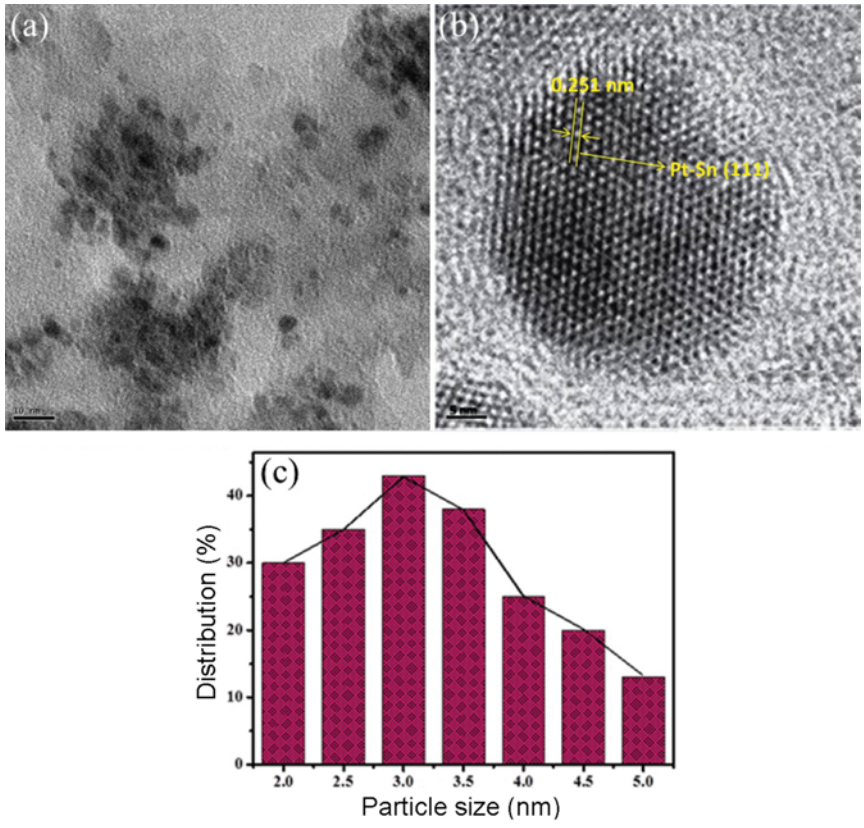

Fig. 4. HRTEM images and size distribution histogram of Pt-Sn/PANI-RHA nanocatalyst.

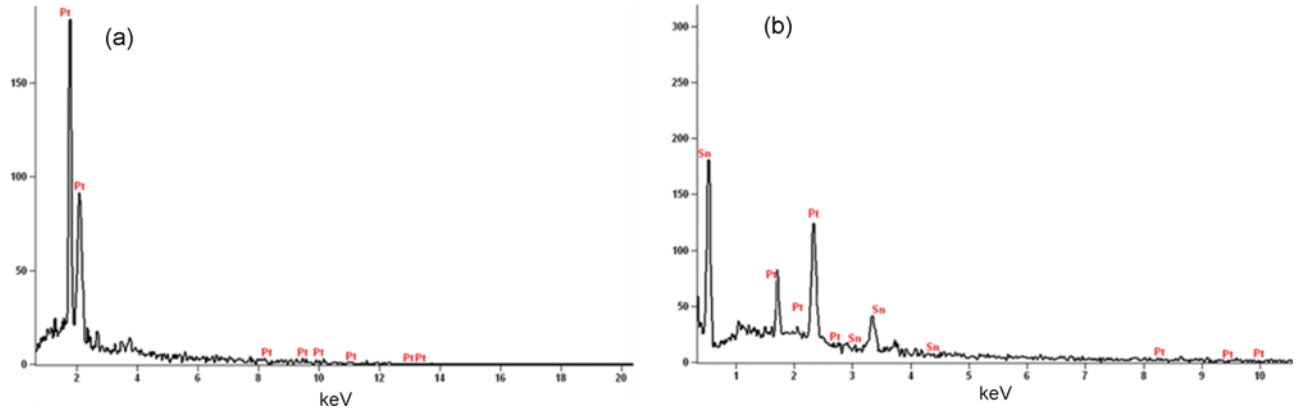

Fig. 5. EDX spectra of (a) Pt/PANI-RHA and (b) Pt-Sn/PANI-RHA nanocatalyst.

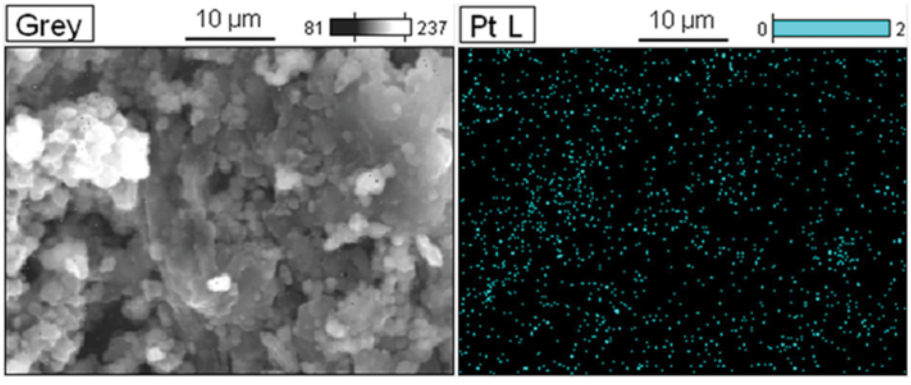

Fig. 6. SEM and EDX mapping pattern of Pt/PANI-RHA nanocatalyst.

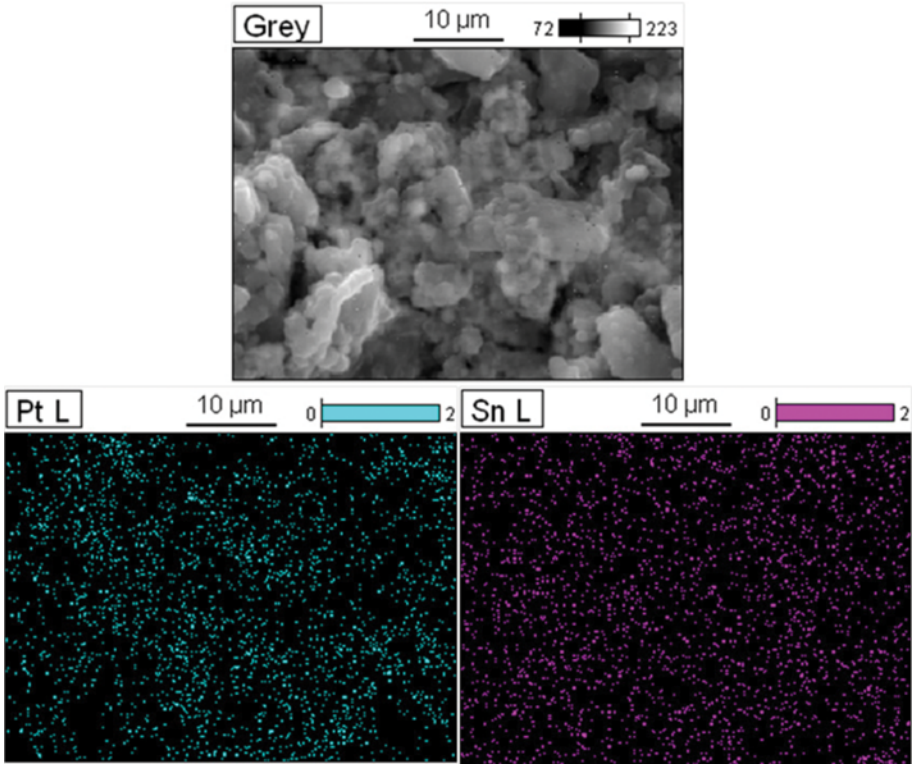

Fig. 7. SEM and EDX mapping pattern of Pt-Sn/PANI-RHA nanocatalyst.

Table 1. Shows atomic and weight composition of Pt and Pt-Sn nanoparticles present on PANI-RHA composite

Nanocatalyst	Weight composition (%)		Atom composition (%)	
	Pt	Sn	Pt	Sn
Pt	100.00	-	100.00	-
Pt-Sn	53.45	46.55	41.33	58.67

tributions of metal nanoparticles on PANI-RHA composite are shown in their respective histograms. The TEM images confirm the spherical and uniform deposition of Pt and Pt-Sn metal nanoparticles on PANI-RHA composite. In the case of Pt-Sn/PANI-RHA, a Pt-Sn alloy was observed as shown in Fig. 4(b). The HRTEM image (Fig. 4(b)) confirms the formation of Pt-Sn bimetal on PANI-RHA surface during the formaldehyde reduction procedure, which was in good agreement with that of the XRD results. The existence of individual metal particles (Pt and Sn) and their contact information were visualized from the TEM picture of the Pt-Sn/PANI-RHA catalyst (Fig. 4(b)). The average particle sizes of Pt and Pt-Sn nanoparticles present on PANI-RHA composite were found to be 2-5 nm. Thus, the improved electrochemical properties for methanol oxidation might be due to the uniform deposition of the particles with small size and bimetallic formation.

4. EDX Analysis

Fig. 5 (a)-(b) shows the EDX pattern of Pt/PANI-RHA and Pt-Sn/PANI-RHA composites. The EDX patterns confirm the presence of Pt and Pt-Sn nanoparticles on PANI-RHA composite. Figs. 6 and 7 show the SEM and EDX mapping images of Pt/PANI-RHA and Pt-Sn/PANI-RHA nanocomposites. The EDX mapping and SEM results confirm the uniform dispersion of Pt and Pt-Sn nanoparticles on PANI-RHA composite. The atomic and weight percentage composition of mono and bimetallic nanoparticles present in PANI-RHA composite are listed in the Table 1. The results were very close to that of experimental value, which demonstrates that metal salts are completely reduced. Further, it affords supporting proof for the existence of metal nanoparticles on PANI-RHA composite.

5. Electrochemical Impedance Spectroscopy

Fig. 8 shows Nyquist plots, which were obtained from electrochemical impedance spectroscopy (EIS) measurements for rice husk ash, poly(aniline) and poly(aniline)-rice husk ash materials. From the results, the electrochemical impedance spectrum of poly(aniline)-rice husk ash has lower charge transfer resistances (R_{ct}) than that of the rice husk ash and poly(aniline) materials. Hence, the conductance of PANI-RHA composite is higher, which provides the evidence for the enhancement of electrooxidation due to the better formation of 3D-structured poly(aniline) on rice husk ash surface [48] and the synergy effect between PANI and RHA in PANI-RHA composite.

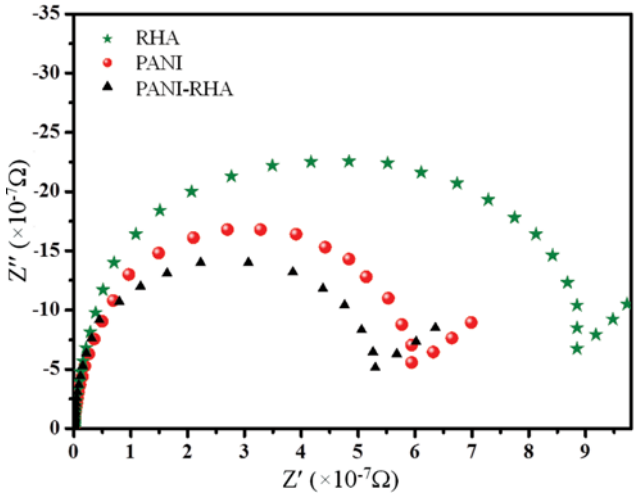

Fig. 8. Nyquist plots of rice husk ash, poly(aniline) and poly(aniline)-rice husk ash materials.

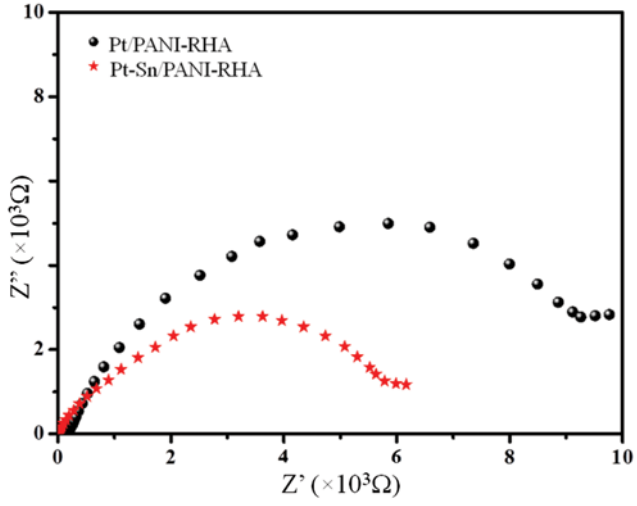

Fig. 9. Nyquist plots of Pt/PANI-RHA and Pt-Sn/PANI-RHA electrocatalysts.

Fig. 9 shows the Nyquist plots of Pt/PANI-RHA and Pt-Sn/PANI-RHA nanocatalyst. The electrochemical impedance spectrum of Pt-Sn/PANI-RHA exhibits lower charge transfer resistance (R_{ct}) than that of the Pt/PANI-RHA nanocatalyst. From the Nyquist plot (Fig. 9), the values of the charge transfer resistances (R_{ct}) are 8.8×10^3 and 5.5×10^3 Ω for Pt/PANI-RHA and Pt-Sn/PANI-RHA nanocatalyst, respectively [48,49]. The smaller charge transfer resistance (R_{ct}) of Pt-Sn/PANI-RHA nanocatalyst also provides supporting evidence that the catalyst can exhibit higher electro-catalytic

Table 2. Intrinsic electron conductivity of rice husk ash, poly(aniline) and rice husk ash-poly(aniline) materials in S/cm at ambient temperature

Sl. No.	Sample	Intrinsic electron conductivity ($\times10^{-3}$ S/cm)
1	Rice husk ash (RHA)	0.1125
2	Polyaniline (PANI)	0.1667
3	Rice husk ash-polyaniline (RHA-PANI)	0.1852

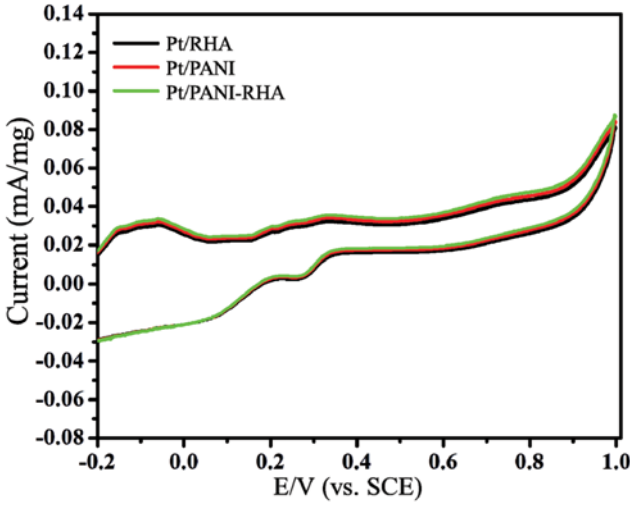

Fig. 10. Cyclic voltammograms of Pt/RHA, Pt/PANI and Pt/PANI-RHA nanocatalysts in 0.5 M H_2SO_4 solution at 50 mVs^{-1}.

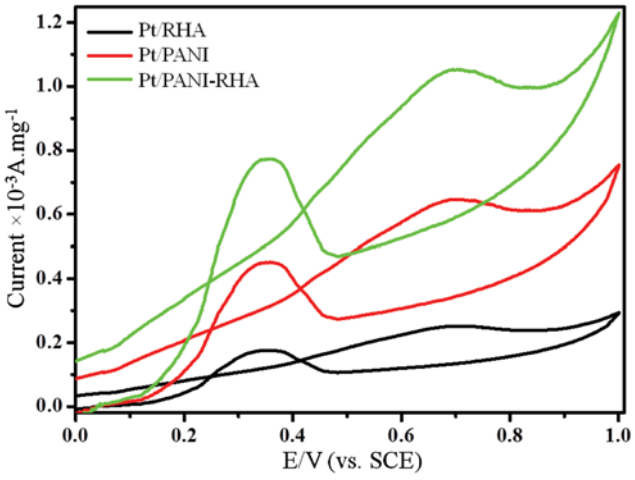

Fig. 11. Cyclic voltammograms of Pt/RHA, Pt/PANI and Pt/PANI-RHA nanocatalysts in 0.5 M H_2SO_4 and 0.5 M CH_3OH solution at 50 mVs^{-1}.

activity for methanol oxidation, which is due to the synergy effect among Pt, Sn and PANI-RHA composite.

6. Intrinsic Electron Conductivity

The electrical conductivities of PANI [50], RHA and PANI/RHA materials were measured according to the standard four-point probe method. The PANI-RHA composite shows enhanced electrical conductivity compared to PANI, which is due to the charge-transfer effect between PANI and RHA. Furthermore, the RHA may serve as conducting bridges, connecting PANI-conducting domains and thus leading to an increase in electron conductivity in PANI-RHA material [51].

7. Cyclic Voltammetry (CV)

Fig. 10 shows the cyclic voltammograms of Pt/RHA, Pt/PANI and Pt/PANI-RHA nanocatalyst in 0.5 M H_2SO_4. From the results, the cyclic voltammograms (CVs) pertaining to Pt nanoparticles modified PANI, RHA and PANI-RHA electrodes overlap in the H_{upd} region, which clearly indicates that the active surface areas for all the electrodes are nearly the same (Fig. 10). The charges and currents associated with the hydrogen adsorption/desorption regions of Pt decorated PANI, RHA and PANI-RHA electrodes were almost the same for all the three electrodes. It is well accepted that two or more electrodes with almost similar currents for the formation and oxidation of adsorbed hydrogen atoms will have exactly the same active surface area of metal [52,53].

The cyclic voltammograms of electrooxidation of methanol on the Pt/RHA, Pt/PANI and Pt/PANI-RHA anodes are shown in Fig. 11. From the results, that the Pt/PANI-RHA composite exhibits higher electro-catalytic activity than that of Pt/PANI and Pt/RHA composites. From Fig. 12, the current increases with an increase in scan rates and a linear relationship (inset figure) was observed between anodic oxidation current and square root of the sweep rate ($\nu^{1/2}$).

These results indicate that the PANI-RHA composite has been found to be a potent supporting material for fuel cell applications, which may be due the synergy effect between PANI, RHA obtained from renewable rice husk waste and platinum nanoparticles in Pt/

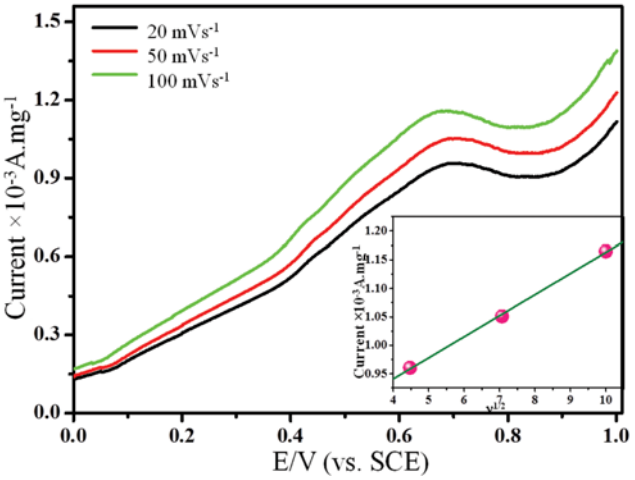

Fig. 12. Effect of scan rate for Pt/PANI-RHA nanocatalyst in 0.5 M H_2SO_4+0.5 M CH_3OH (scan rate=20, 50 and 100 mVs^{-1}). The inset graph shows the dependence of the anodic oxidation current on the square root of scan rates.

PANI-RHA composite. Hence, this will reduce the overall cost of the materials for commercialization of alcohol fuel cells. Furthermore, the present work is focused on reducing the quantity of high priced platinum catalyst by alloying with low cost tin metal. So, the cyclic voltammetry measurements were carried out for Pt/PANI-RHA and Pt-Sn/ PANI-RHA nanocatalysts in 0.5 M H_2SO_4 (Fig. 13). Fig. 14 illustrates the cyclic voltammograms of electrooxidation of methanol on Pt/PANI-RHA and Pt-Sn/PANI-RHA anodes in 0.5 H_2SO_4 and 0.5 methanol at 50 mVs^{-1}.

From the result (Fig. 14), Pt-Sn/PANI-RHA catalyst shows enhanced catalytic activity compared to that of Pt/PANI-RHA catalyst. The possible proposed mechanism has been shown in Scheme 2, which explains how the tin would enhance the electrocatalytic activity of the methanol oxidation. This is because the methanol oxidation takes place on Pt nanoparticles with the formation of CO poison as a byproduct, which reduces the catalytic activity of

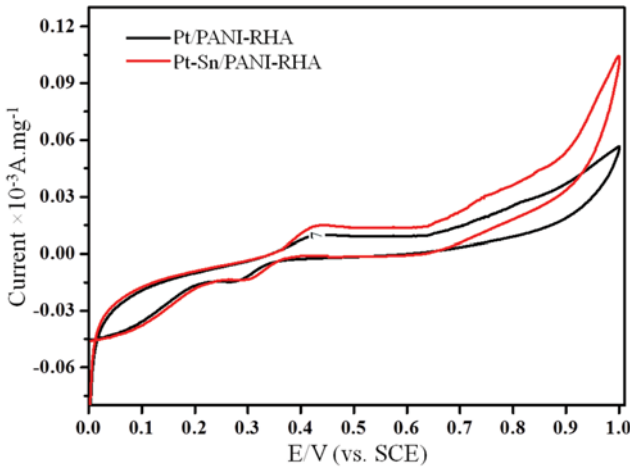

Fig. 13. Cyclic voltammograms of Pt/PANI-RHA and Pt-Sn/ PANI-RHA nanocatalysts in 0.5 M H_2SO_4 solution at a scan rate of 50 mVs^{-1}.

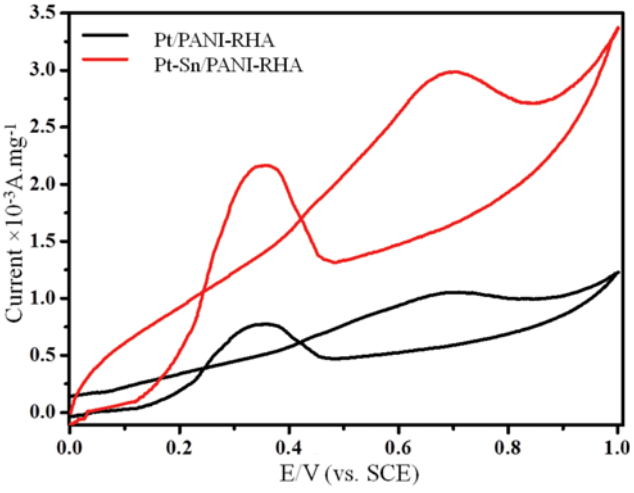

Fig. 14. Cyclic voltammograms of Pt/PANI-RHA and Pt-Sn/PANI-RHA nanocatalysts in 0.5 M H_2SO_4 and 0.5 M CH_3OH solution at 50 mVs^{-1}.

Pt catalyst [54]. So, as already identified, the pure platinum does not act as good anode catalyst for methanol oxidation because of strongly adsorbed 'CO' intermediates as catalytic poison that will reduce the active surface of the platinum (Scheme 2).

However, the addition of tin with platinum can promote the CO oxidation at a lower potential than that of Pt, which will enhance the electrocatalytic activity towards methanol oxidation. Thus, the addition of tin acts as promoter to oxidize 'CO' poisoning intermediate formed on a platinum surface during methanol oxidation. The OH_{ads} adsorbed on the metallic tin can be obtained by the activation of water molecules at a lower potential than that of Pt [55]. The adsorption of OH on Sn is easier than that of Pt

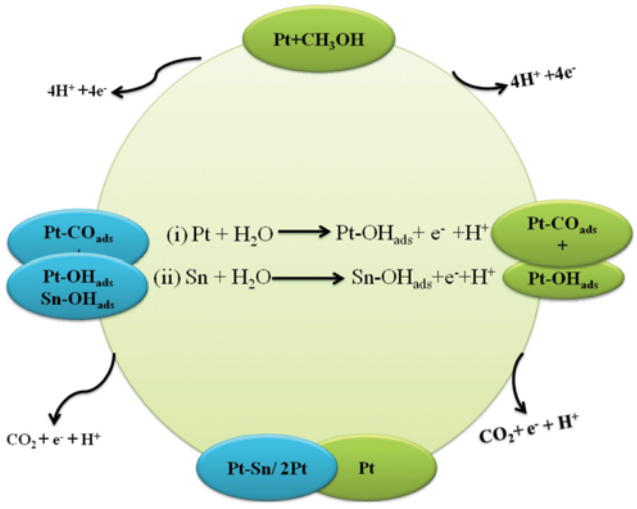

Scheme 2. The schematic representation of CH_3OH oxidation on Pt/PANI-RHA and Pt-Sn/PANI-RHA composites.

through water activation, which is a key to oxidizing the adsorbed CO poison on the electrode and hence more predominately in Pt-Sn than that of Pt nanoparticles. This implies that the CO oxidation on Pt-Sn/PANI-RHA composite needs less potential than that of Pt/PANI-RHA composite through the water activation process. Though the difference in the onset potential values of Pt/PANI-RHA and Pt-Sn/PANI-RHA electrodes is very small (0.35 for Pt and 0.32 V for Pt-Sn), the synergy effect between Pt, Sn and PANI-RHA composite enhances the catalytic activity, which is in good agreement with that of previous reports [56,57]. Further the addition of Sn with platinum can increase the distance between the two adjacent Pt atoms, which reduces the adsorption of CO on its surface through bi-functional mechanism [58].

Pt-Sn/PANI-RHA composite (Table 3) displays higher catalytic activity compared to that of Pt/PANI-RHA composite, due to the lower activation energy required for hydrolysis of water molecules on Pt-Sn that is essential for the oxidation of CO poison molecules. The anodic oxidation current of Pt-Sn/PANI-RHA is about three-times higher than that of Pt/PANI-RHA. Hence, Pt-Sn/PANI-RHA composite has proven to be a potent and low-cost nanocatalyst, which has been synthesized successfully for methanol fuel cell applications. The decreasing order of the electrocatalytic activity of the nanocatalyst for methanol oxidation is Pt-Sn/PANI-RHA (2.983 mA)>Pt/PANI-RHA (1.053 mA)>Pt/PANI (0.651 mA)> Pt/RHA (0.248 mA).

The ratio of the forward anodic peak to the backward peak current density (I_f/I_b) relates to the ability of the catalyst to tolerate carbonaceous species, [59-61] and thus it should generally be a higher value for the best-performing catalyst. From the cyclic voltammograms, the I_f/I_b ratios are 1.21 and 1.38 for Pt/PANI-RHA and Pt-Sn/PANI-RHA electrocatalyst, respectively. The results indi-

Table 3. Anodic oxidation current of Pt/RHA, Pt/PANI, Pt/PANI-RHA and Pt-Sn/PANI-RHA nanocatalysts for methanol oxidation

Nanocatalyst	Pt/RHA	Pt/PANI	Pt/PANI-RHA	Pt-Sn/PANI-RHA
Anodic oxidation current (10^{-3} A·mg^{-1})	0.248	0.651	1.053	2.983

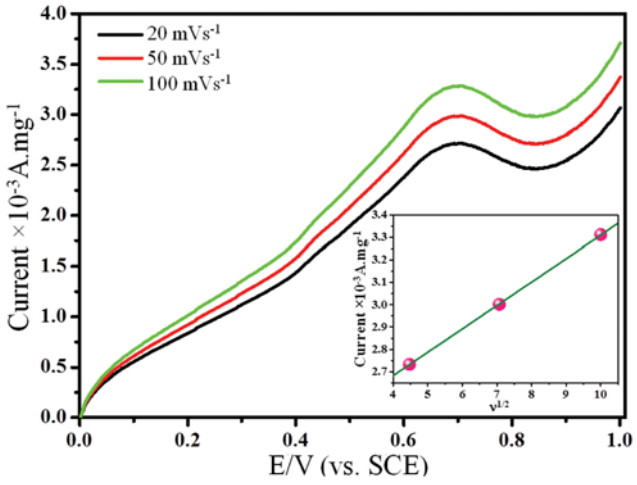

Fig. 15. Effect of scan rate for Pt-Sn/PANI-RHA nanocatalysts in 0.5 M H_2SO_4+0.5 M CH_3OH (scan rate=20, 50 and 100 mVs^{-1}). The inset graph shows the dependence of the anodic oxidation current on the square root of scan rates.

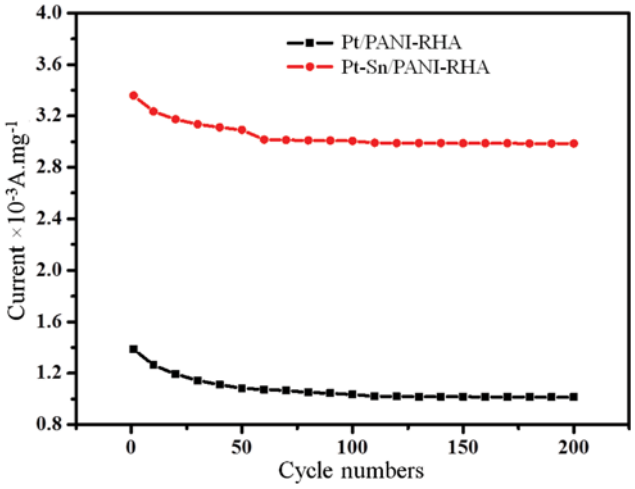

Fig. 17. Long-term stability of Pt/PANI-RHA and Pt-Sn/PANI-RHA nanocatalysts in 0.5 M H_2SO_4 and 0.5 M CH_3OH solution at 50 mVs^{-1}.

cate that Pt-Sn/PANI-RHA electrocatalyst shows better catalytic poison tolerance through bi-functional effect than that of Pt/PANI-RHA electrocatalyst, which indicates that Pt-Sn/PANI-RHA exhibits its lower accumulation of CO-like species during the methanol oxidation reaction, thus leading to excellent catalytic activity [62].

The effect of scan rate was carried out in Pt-Sn/PANI-RHA nanocatalyst to characterize the transport properties of methanol during electrooxidation (Fig. 15). From Fig. 15, the anodic oxidation current increases consistently with increasing the scan rates. Furthermore, a linear relationship was observed from the plot between anodic oxidation current obtained from forward CV scans and the square root of different sweep rate ($\nu^{1/2}$) is shown as inset figure, which implies that the electrooxidation of methanol on Pt-Sn/PANI-RHA nanocatalyst is a diffusion controlled process [63].

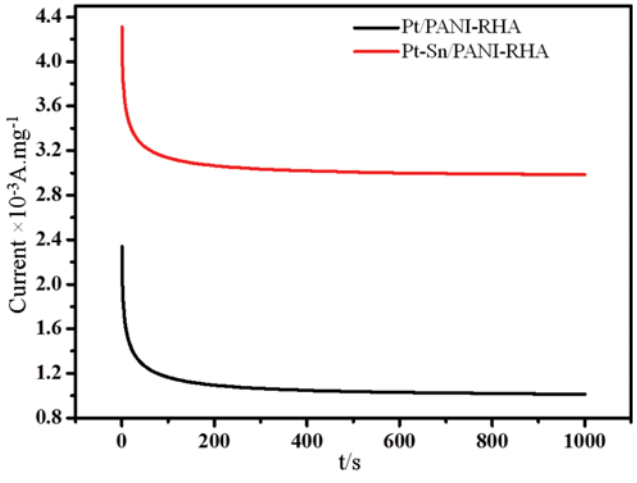

Fig. 16. Chronoamperometric curves for Pt/PANI-RHA and Pt-Sn/PANI-RHA nanocatalysts in 0.5 M H_2SO_4 and 0.5 M CH_3OH solution at a potential of 50 mVs^{-1}.

8. Chronoamperometric Analysis (CA)

Additionally, chronoamperometry analysis and long-term stability have been carried out to investigate the electrocatalytic activity and stability of Pt/PANI-RHA and Pt-Sn/PANI-RHA nanocatalysts. From the result (Fig. 16), it has been noticed that the steady state current decreased initially, which may be due to the double-layer charge and the formation of carbonaceous intermediates during methanol oxidation. After a few seconds, a constant steady state current was observed for both the nanocatalysts, which is in good agreement with the current observed from cyclic voltammetry studies. Thus, Pt/PANI-RHA and Pt-Sn/PANI-RHA nanocatalysts show good electrocatalytic performance and stability, which is due to the uniform distribution of metal nanoparticles and chemical interaction between metal nanoparticles and PANI/RHA composite.

9. Long-term Stability

The long-term cycle stability of the nanocatalyst is essential for practical applications, which was examined by CV in 0.5 M H_2SO_4 and 0.5 M CH_3OH solutions at 50 mV s^{-1} and their results are shown in Fig. 17. In Fig. 17, the anodic oxidation current's gradual decrease with the consecutive scan is due to the dissolution of adsorbed metal nanoparticles from the PANI-RHA matrix and the formation of carbonaceous intermediate during the methanol oxidation. The anodic oxidation currents at 200 cycles are about 73.1% and 89.5% with respect to the first cycle of Pt/PANI-RHA and Pt-Sn/PANI-RHA nanocatalysts. This ensures that Pt-Sn/PANI-RHA composite can have maximum stability compared to that of other Pt/PANI-RHA.

CONCLUSIONS

Highly dispersed Pt and Pt-Sn nanoparticles on poly(aniline)-rice husk ash composite were synthesized by the $NaBH_4$ reduction method for methanol oxidation. The synthesized materials were characterized by various analytical techniques. The HR-TEM, SEM and EDX mapping studies confirm the uniformly dis-

persed metal nanoparticles on PANI-RHA surface. EIS images reveal that the PANI-RHA has a lower charge transfer resistance value than that of the PANI and RHA, which is due to the 3D polyaromatic structure of aniline on RHA surface and the small charge transfer resistance value for Pt-Sn/PANI-RHA nanocatalyst. These studies can provide the supporting evidence for its higher catalytic activity towards methanol oxidation. The results indicate that Pt-Sn/PANI-RHA nanocatalyst has a much higher electrocatalytic activity than that of Pt/PANI-RHA nanocatalyst. The chronoamperometric and long-term stability analyses confirm the stability of metal nanoparticles supported on PANI-RHA composite. Hence, Pt-Sn/PANI-RHA is a potent electrocatalyst for methanol oxidation, which is due to excellent electrocatalytic activity and stability.

ACKNOWLEDGEMENT

The authors would like to thank DST/Nanomission, New Delhi, India for the financial support to carry out this work and the establishment of Nanotech Research Lab through the grant No. SR/NM/NS-05/2011(G).

REFERENCES

1. Y. H. Lee, G. Lee, J. H. Shim, S. Hwang, J. Kwak, K. Lee, H. Song and J. T. Park, *Chem. Mater.*, **18**, 4209 (2006).
2. H. Q. Song, P. Xiao, X. P. Qiu and W. T. Zhu, *J. Power Sources*, **195**, 1610 (2010).
3. Y. C. Zhao, F. Y. Wang, J. N. Tian, X. L. Yang and L. Zhan, *Electrochim. Acta*, **55**, 8998 (2010).
4. V. Selvaraj, M. Alagar and I. Hamerton, *J. Power Sources*, **160**, 940 (2006).
5. V. Selvaraj and M. Alagar, *Electrochem. Commun.*, **9**, 1145 (2007).
6. H. B. Hassan, *J. Fuel Chem. Technol.*, **37**, 346 (2009).
7. C.-T. Hsieh and J.-Y. Lin, *J. Power Sources*, **188**, 347 (2009).
8. M. Rahsepar, M. Pakshir, Y. Piao and H. Kim, *Electrochim. Acta*, **71**, 246 (2012).
9. N. V. Long, T. D. Hien, T. Asaka, M. Ohtaki and M. Nogami, *Int. J. Hydrogen Energy*, **36**, 8478 (2011).
10. A. T. Ezhil Vilian, S.-M. Chen and S. Piraman, *New J. Chem.* (2015), DOI:10.1039/C4NJ01470G.
11. J. Yuan, B. He, L. Hong, J. Lu, J. Miao and L. Niu, *J. Mater. Chem.*, **22**, 19658 (2012).
12. F. Ren, C. Wang, C. Zha, F. Jiang, R. Yue, Y. Du, P. Yang and J. Xu, *J. Mater. Chem. A*, **1**, 7255 (2013).
13. C. KokPoh, Z. Tian, J. Gao, Z. Liu, J. Lin, Y. P. Feng and F. Su, *J. Mater. Chem.*, **22**, 13643 (2012).
14. N. Tsiouvaras, M. V. Martínez-Huerta, O. Paschos, U. Stimming, J. L. G. Fierro and M. A. Peña, *Int. J. Hydrogen Energy*, **35**, 11478 (2010).
15. X. Zhang, F. Zhang, R.-F. Guan and K.-Y. Chan, *Mater. Res. Bull.*, **42**, 327 (2007).
16. M. P. Hogarth and T. R. Ralph, *Met. Rev.*, **46**, 146 (2002).
17. M. Uchida, Y. Aoyama, M. Tanabe, N. Yanagihara, N. Eda and A. Ohta, *J. Electrochem. Soc.*, **142**, 2572 (1995).
18. G. Wu, Y. S. Chen and B. Q. Xu, *Electrochem. Commun.*, **7**, 1237 (2005).
19. F. Adam, P. Retnam and A. Iqbal, *Appl. Catal. A*, **357**, 93 (2009).
20. F. Adam and C. L. Fook, *J. Porous Mater.*, **16**, 291 (2009).
21. F. Adam, K. Kandasamy and S. Balakrishnan, *J. Colloid Interface Sci.*, **304**, 137 (2006).
22. F. Adam and A. E. Ahmed, *Chem. Eng. J.*, **145**, 328 (2008).
23. R. H. Friend, R. W. Gymer, A. B. Holmes, J. H. Burroughes, R. N. Marks, C. Taliani, D. D. C. Bradley, D. A. Dos Santos, J. L. Bredas, M. Logdlund and W. R. Salaneck, *Nature*, **397**, 121 (1999).
24. C. D. Muller, A. Falcou, N. Reckefuss, M. Rojahn, V. Wiederhirn, P. Rudati, H. Frohne, O. Nuyken, H. Becher and K. Meerholz, *Nature*, **421**, 829 (2003).
25. H. Sirringhuas, N. Tessler and R. H. Friend, *Science*, **280**, 1741 (1998).
26. C. D. Dimitrakopoulos and D. J. Mascaro, *J. Res. De.*, **45**, 11 (2001).
27. G. Yu, J. Gao, J. C. Hummelen, F. Wudl and A. J. Heeger, *Science*, **270**, 1789 (1995).
28. C. J. Brabec, N. S. Sariciftci and J. C. Hummelen, *Adv. Funct. Mater.*, **11**, 15 (2001).
29. P. Malkaj, E. Dalas, E. Viteratos and S. Sakkopoulos, *J. Appl. Polym. Sci.*, **101**, 1853 (2006).
30. Y. C. Luo and J. S. Do, *Sens. Actuators B*, **115**, 102 (2009).
31. A. G. MacDiarmid, S. L. Mu, N. L. D. Somasiri and W. Wu, *Mol. Cryst. Liq. Cryst.*, **121**, 173 (1985).
32. T. Koboyashi, H. Yoneyama and H. Tamura, *J. Electroanal. Chem.*, **177**, 281 (1984).
33. D. Sazou and D. Kosseoglou, *Electrochim. Acta*, **51**, 2503 (2006).
34. B. Habibi, M. H. Pournaghi-Azar, H. Abdolmohammad-Zadeh and H. Razmi, *Int. J. Hydrogen Energy*, **34**, 2880 (2009).
35. C. Arbizzani, M. Biso, E. Manferrari and M. Mastragostino, *J. Power Sources*, **178**, 584 (2008).
36. S. Patra and N. Munichandraiah, *Langmuir*, **25**, 1732 (2009).
37. K. K. Tintula, S. Pitchumani, P. Sridhar and A. K. Shukla, *J. Chem. Sci.*, **122**, 381 (2010).
38. J. Yano, T. Shiraga and A. Kitani, *J. New Mater. Electrochem. Syst.*, **11**, 235 (2008).
39. A. Imyim and E. Prapalimrungsi, *J. Hazard. Mater.*, **184**, 775 (2010).
40. M. Ghorbani and H. Eisazadeh, *Compos. Part B-Eng.*, **45**, 1 (2013).
41. M. Ghorbani and H. Eisazadeh, *Synt. Met.*, **162**, 527 (2012).
42. M. Ghorbani, M. S. Lashkenari and H. Eisazadeh, *Synt. Met.*, **161**, 1430 (2011).
43. M. Ghorbani, H. Eisazadeh and A. A. Ghoreyshi, *IJEE*, **3**, 83 (2012).
44. W. Li, W. Zhou, H. Li, Z. Zhou, B. Zhou, G. Sun and Q. Xin, *Electrochim. Acta*, **49**, 1045 (2004).
45. C. He, H. R. Kunz and J. M. Fenton, *J. Electrochem. Soc.*, **144**, 970 (1997).
46. F. Colmati, E. Antolini and E. R. Gonzalez, *Electrochim. Acta*, **50**, 5496 (2005).
47. W. Zhou, Z. Zhou, S. Song, W. Li, G. Sun, P. Tsiakaras and Q. Xin, *Appl. Catal. B*, **46**, 273 (2003).
48. A. Ali Ensafi, Mehdi Jafari-Asl and Behzad Rezaei, *Electrochim. Acta*, **130**, 397 (2014).
49. H. Cao, Z. Fan, G. Hou, Y. Tang and G. Zheng, *Electrochim. Acta*, **125**, 275 (2014).
50. H. C. Pant, M. K. Patra, S. C. Negi, A. Bhatia, S. R. Vadera and N. Kumar, *Bull. Mater. Sci.*, **29**, 379 (2006).

51. S. I. A. Razak, A. L. Ahmad, S. H. S. Zein and A. R. Boccaccini, *Script. Mater.*, **61**, 592 (2009).
52. Y. M. Wu, W. S. Li, J. Lu, J. H. Du, D. S. Lu and J. M. Fu, *J. Power Sources*, **145**, 286 (2005).
53. L. H. Mascaro, M. C. Santos, S. A. S. Machado and L. A. Avac, *J. Braz. Chem. Soc.*, **13**, 529 (2002).
54. J. Wang, R. Shi, X. Guo, J. Xi, J. Zhao, C. Song, L. Wang and J. Zhang, *Electrochim. Acta*, **123**, 309 (2014).
55. M. Seruga, M. Metikos-Hukovic, T. Valla, M. Milun, H. Hoffschultz and K. Wandelt, *J. Electroanal. Chem.*, **407**, 83 (1996).
56. X. W. Yu and P. G. Pickup, *J. Power Sources*, **182**, 124 (2008).
57. F. Colmati, E. Antolini and E. R. Gonzalez, *Electrochim. Acta,* **50**, 549 (2005).
58. F. Han, X. Wang, J. Lian and Y. Wang, *Carbon,* **50**, 5498 (2012).
59. X. Yang, Q. Yang, J. Xu and C.-S. Lee, *J. Mater. Chem.,* **22**, 8057 (2012).
60. B. Wu, B. Wang, C. Deng and Y. Gao, *Appl. Catal., B,* **103**, 163 (2011).
61. Y.-W. Lee, A.-R. Ko, S.-B. Han, H.-S. Kim and K.-W. Park, *Phys. Chem. Chem. Phys.*, **13**, 5569 (2011).
62. A. T. Ezhil Vilian, S.-M. Chen and S. Piraman, *New J. Chem.*, **39**, 953 (2015).
63. M. Watanabe and S. Motoo, *J. Electroanal. Chem.*, **60**, 275 (1975).